Heterogeneities in the glassy state

Katharina Vollmayr-Lee[1,2,*] and Annette Zippelius[2]
[1]*Department of Physics, Bucknell University, Lewisburg, Pennsylvania 17837, USA*
[2]*Institut für Theoretische Physik, Universität Göttingen, Friedrich-Hund-Platz 1, D-37077 Göttingen, Germany*
(Received 5 July 2005; published 20 October 2005)

We study heterogeneities in a binary Lennard-Jones system below the glass transition using molecular dynamics simulations. We identify mobile and immobile particles and measure their distribution of vibrational amplitudes. For temperatures near the glass transition the distribution of vibrational amplitudes obeys scaling and compares reasonably well with a mean-field theory for the amorphous solid state. To investigate correlations among the immobile and mobile particles we identify clusters and analyze their size and shape. For a fixed number of immobile particles we observe that the immobile particles cluster more strongly together as the temperature is increased which allows the particles to block each other more effectively and to therefore stay immobile. For the mobile particles, on the other hand, the clustering is most pronounced at low temperatures, indicating that mobility at low temperatures can only be sustained in cooperative motion.

DOI: 10.1103/PhysRevE.72.041507 PACS number(s): 64.70.Pf, 02.70.Ns, 61.43.Fs

I. INTRODUCTION

If a liquid is cooled and crystallization is avoided, one obtains a supercooled liquid. Upon further cooling the system falls out of equilibrium and results in an amorphous solid—i.e., a glass. During this transition from liquid to supercooled liquid to glass the dynamic properties change drastically and they therefore have received much attention. Most studies are concerned with the supercooled liquid, for which the existence of dynamic heterogeneities has been well established [1]. We focus in this paper instead on the *glass* phase.

The glassy state of matter is by definition strongly inhomogeneous. Different particles have different neighborhoods and consequently different dynamics. One tool to diagnose the heterogeneities are the vibrational amplitudes $\langle d_i^2 \rangle$. In contrast to a perfect crystal these vary strongly from site to site in the glassy state. A simple way to demonstrate the heterogeneities is to pick out the 5% particles which have the smallest and largest amplitudes. Their vibrational amplitudes are plotted in Fig. 1 for a binary Lennard-Jones mixture (for details see below). The most striking observation is the spread in the data which strongly increases with increasing temperature. Whereas for $T=0.15$ the $\langle d_i^2 \rangle$ of the 5% fastest particles is approximately 5 times the $\langle d_i^2 \rangle$ of the 5% slowest particles, this grows to a factor of approximately 50 close to the glass transition temperature. Thus, heterogeneities are present in the glassy state for all temperatures and become increasingly more pronounced as the glass transition temperature is approached from below.

Our goal is to characterize these heterogeneities quantitatively. Obviously the mean of the vibrational amplitudes is not conclusive and we therefore investigate instead the full distribution of vibrational amplitudes to characterize the local dynamics. We compute this distribution and show that, in the vicinity of the glass transition, it approximately obeys scaling. We furthermore compare it to a mean-field calculation for a different amorphous solid [2,3], the gel, and find surprisingly good agreement.

To further characterize dynamic as well as time-persistent heterogeneities we use various definitions to identify mobile and immobile particles. We identify clusters of immobile and mobile particles where particles are defined to be connected if their relative distance is smaller than the position of the first minimum of the pair correlation function. To quantify the shape of these clusters we analyze their connectivity properties in analogy to covalently bonded glasses. We determine the average size of the clusters, the average coordination number, and the spatial extent as measured by the radius of gyration. In addition to the average values we also compute the distribution of coordination numbers as well as ring statistics.

The majority of previous work on dynamic heterogeneities are studies of *mobile* particles *above* the glass transition.

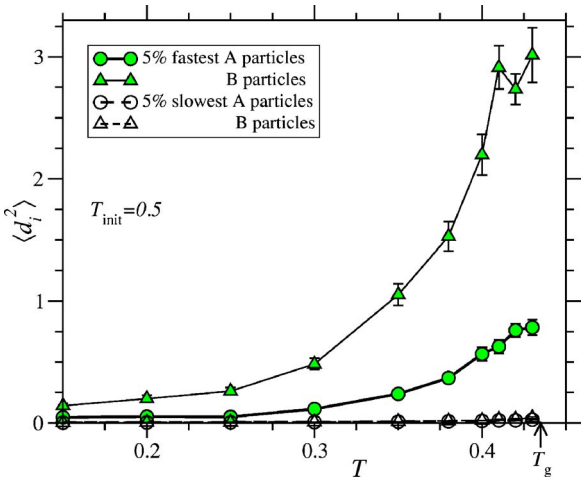

FIG. 1. (Color online) Vibrational amplitude $\langle d_i^2 \rangle$ as a function of temperature for the 5% fastest and 5% slowest particles. See Fig. 5 for an enlargement of $\langle d_i^2 \rangle(T)$ for the 5% slowest *A* and *B* particles.

*Electronic address: kvollmay@bucknell.edu

They find that mobile particles form stringlike clusters [4–8] which grow in length and size with decreasing temperature [9–11]. Immobile particles, on the other hand, do not form strings [5,6]. In this paper we mostly study clusters of *immobile* particles *below* the glass transition and quantify their size and shape as described above.

The paper is organized as follows. In Sec. II we give details of the simulation. Subsequently several different definitions of immobile particles are introduced and discussed (Sec. III). In Sec. IV we present our results, first for the fraction of immobile particles (A), next for the vibrational amplitudes (B), and finally the cluster analysis (C). We summarize our results and present conclusions in Sec. V.

II. SIMULATION DETAILS

Our system is a binary Lennard-Jones mixture of 800 A and 200 B particles with the same mass. The interaction potential between particles i and j of type $\alpha,\beta \in \{A,B\}$ and at positions $\mathbf{r}_i$ and $\mathbf{r}_j$ is

$$V_{\alpha\beta}(r) = 4\epsilon_{\alpha\beta}\left[\left(\frac{\sigma_{\alpha\beta}}{r}\right)^{12} - \left(\frac{\sigma_{\alpha\beta}}{r}\right)^{6}\right], \tag{1}$$

where $r=|\mathbf{r}_i-\mathbf{r}_j|$ and $\epsilon_{AA}=1.0$, $\epsilon_{AB}=1.5$, $\epsilon_{BB}=0.5$, $\sigma_{AA}=1.0$, $\sigma_{AB}=0.8$, and $\sigma_{BB}=0.88$. We truncate and shift the potential at $r=2.5\sigma_{\alpha\beta}$. From previous investigations [12] it is known that this system is not prone to crystallization and demixing. In the following we will use reduced units where the unit of length is σ_{AA}, the unit of energy is ϵ_{AA}, and the unit of time is $\sqrt{m\sigma_{AA}^2/(48\epsilon_{AA})}$.

We carry out molecular dynamics (MD) simulations using the velocity Verlet algorithm with a time step of 0.02. The volume is kept constant at $V=9.4^3=831$, and we use periodic boundary conditions. Previous simulations [12] showed that the system falls out of equilibrium in the vicinity of $T_g=0.435$. We are interested in the glassy phase and hence study the system well below and close to this temperature in the range $0.15 \leqslant T \leqslant 0.43$.

As described in Sec. IX of [13] we equilibrate the system at constant temperature $T=3.0$ to obtain ten independent configurations which are at least 5×10^4 time units apart. This corresponds to about 10^4 times longer than the longest relaxation time determined at $T=3.0$ (see [12]). The temperature is kept constant by replacing the velocities of all particles by new velocities drawn from the corresponding Boltzmann distribution every 50 time steps. Each of these configurations is then cooled linearly in time t [$T(t)=T_0-\gamma t$] from $T_0=3.0$ to $T_{\text{init}}=0.5$ with $\gamma=1.25\times10^{-5}$ [14]. After an (NVT) equilibration at $T=0.5$ of 2×10^5 time units (corresponding to about 100 times the longest relaxation time [12]) we then instantaneously quench the system to the investigated temperatures $T=0.15$, 0.20, 0.25, 0.30, 0.35, 0.38, 0.40, 0.41, 0.42, and 0.43. We anneal the system at each temperature with (NVT) simulations for 2000 time units and then run the production runs with (NVE) simulations for 10^5 time units. Since the relaxation times τ are much larger than the waiting time before the production runs ($\tau \approx 8\times10^5$ at $T=0.446$), we expect to find aging effects as they have been studied in detail for the same Lennard-Jones system [16,17] and as they have been found in related work [13,18]. In this paper we do not aim for a systematic investigation of aging effects. However, we have analyzed a second set of simulation runs with a different history in order to get a rough estimate of the effects of aging. The second set of runs start from well equilibrated configurations at $T_{\text{init}}=0.446$. After an instantaneous quench to $T=0.15$ the system is annealed for 2000 time units followed by a (NVT) run of also 2000 time units. The temperature is then raised to $T=0.2$, again annealed with (NVT) and (NVE) runs each of 2000 time units, and raised to $T=0.25$ etc. The production runs are for 10^5 time units and are for each investigated temperature following the respective (NVE) simulations. For more details see [13,18]

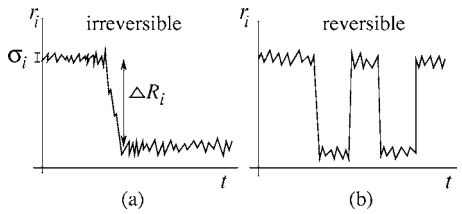

FIG. 2. Sketch of a particle trajectory to illustrate the definition of irreversible and reversible jumps.

III. DEFINITION OF IMMOBILE AND MOBILE PARTICLES

We study heterogeneities below the glass transition and focus on how the particles are increasingly frozen in as the temperature is lowered. Even though the system is obviously very inhomogeneous (see Sec. I), it is not obvious how to quantify the characteristic features of these heterogeneities. One possibility is to study the extremes, the most mobile and the most immobile particles. In most of this paper we concentrate on the immobile ones; we study their organization into clusters and the size and shape of these clusters.

Using four different definitions of immobility we are able to test if the resulting dynamical behavior is dependent on the precise definition of immobility. For two of the definitions we characterize the mobility of a particle by its vibrational amplitude [18]

$$d_i^2 = \overline{|\mathbf{r}_i - \bar{\mathbf{r}}_i|^2}, \tag{2}$$

where the overbar denotes a time average over the whole simulation run. Our first definition of immobility (I) defines every particle i to be immobile for which

$$d_i^2 \leqslant d_{\text{cut}}^2. \tag{3}$$

The second definition of immobility (II) [18] identifies as immobile particles a fixed percentage of A particles and separately a fixed percentage of B particles with the smallest d_i^2. This allows us to similarly study the most mobile particles with the largest d_i^2.

The third and fourth definitions of immobility are based on recent work on single-particle motion [13]. As sketched in Fig. 2(a), we define a particle i to undergo a jump if its

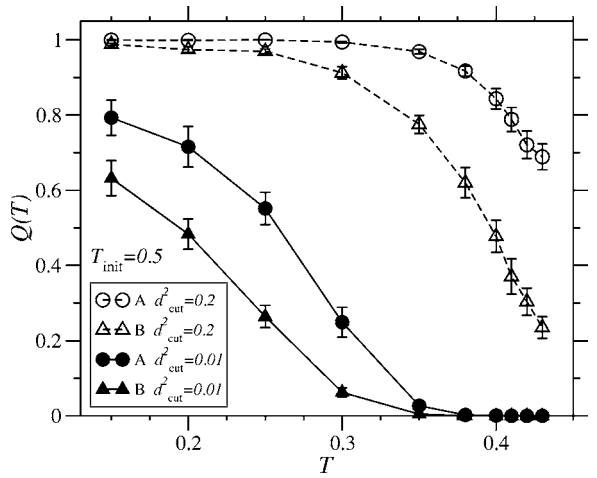

FIG. 3. The fraction of immobile particles Q as a function of temperature T using definition I for immobility. $Q(T)$ is given both for A and B particles separately and for $d^2_{\mathrm{cut}}=0.2$ and $d^2_{\mathrm{cut}}=0.01$. The simulations are with initial temperature $T_{\mathrm{init}}=0.5$.

change in average position ΔR_i is significantly larger than its fluctuation σ_i ($\Delta R_i > \sqrt{20}\sigma_i$) [19]. We distinguish irreversible and reversible jumps where in the latter case the particle returns during the simulation run to one of its former average positions (for more details see [13]). We call all particles immobile which are not undergoing any jumps (III) or which are not irreversible jumpers (IV).

Note that our definitions of immobile particles refer to the whole simulation run, because we want to investigate those structures which persist on the longest time scale, set by the length of the simulation run.

IV. RESULTS

A. Fraction of immobile particles

Let us first see how many particles are immobile according to the definitions I, III, and IV. Figures 3 and 4 show that the fraction of immobile particles,

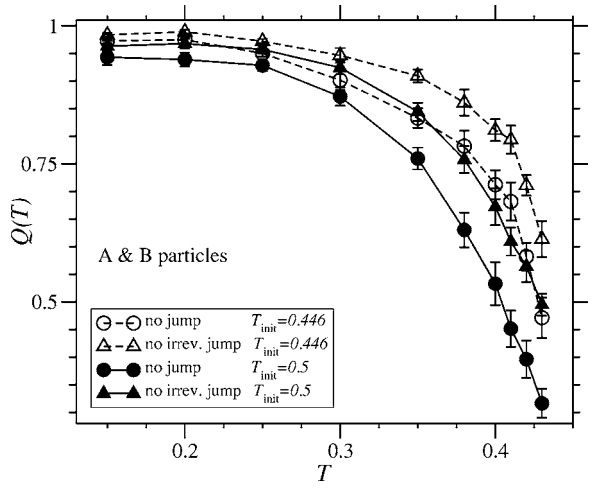

FIG. 4. Same as Fig. 3, but for definitions III and IV, for A and B particles and for different initial temperatures.

$$Q = (\text{number of immobile particles})/(\text{number of particles}), \tag{4}$$

approaches 1 for very low temperatures and drops significantly for temperatures near the glass transition. $Q(T)$ depends quantitatively on the definition of immobile: the larger d^2_{cut}, the steeper is the drop of Q. The smallest cutoff $d^2_{\mathrm{cut}}=0.01$ corresponds to the Lindemann criterion and gives rise to significant deviations in the results for $Q(T)$ as compared to the other definitions of immobility. Apparently the frozen structure can be sustained with a considerable fraction of particles whose vibrational amplitude is larger than suggested by the Lindemann criterion—e.g., roughly 25% of the A particles at $T=0.3$. This is consistent with the broad scatter of vibrational amplitudes in the glassy phase that we shall discuss below.

The qualitative behavior is the same for all definitions of immobility and in particular the temperature where Q goes to zero is rather insensitive to the details of the definition of immobile particles (unless the cutoff is chosen too small; see above). Hence Q gives a rough estimate of T_{g} via the extrapolation of $Q(T)$ to zero. Similarly the history of the simulation runs has a quantitative influence on $Q(T)$: larger initial temperature ($T_{\mathrm{init}}=0.5$) results in fewer immobile particles, consistent with Fig. 22 of [13]. The qualitative behavior, however, is not only independent of the precise definition of immobility but also independent of the history of the simulation runs.

B. Vibrational amplitude

One possibility to extract the various length scales of the glassy state is the vibrational amplitudes $\{d_i^2\}$. Figure 1 shows $\langle d_i^2\rangle$ as a function of temperature T for the 5% particles with largest d_i^2 (mobile, solid symbols) and the 5% particles with smallest d_i^2 (immobile, open symbols). Here $\langle\cdot\rangle$ denotes an average over the subset of particles under consideration (mobile or immobile) and over initial configurations [20]. The remarkable spread of $\langle d_i^2\rangle$ in Fig. 1 illustrates the increasing importance of heterogeneities when the glass transition temperature is approached from below (see Sec. I). In the inset of Fig. 5 we have included linear fits through the origin, which would correspond to the dynamics of a harmonic solid. We find for the 5% immobile particles $\langle d_i^2\rangle(T)$ for $T \leqslant 0.25$ good agreement with this line fit. For larger temperatures, however, the immobile particles display anharmonic dynamics. On the other hand, the immobile particles of definitions I, III, and IV include at low temperatures almost all particles (see Figs. 3 and 4), and the linear fits through the origin are therefore only good approximations for $T \leqslant 0.2$ which corresponds roughly to the crossing of the line of the Lindemann criterion (see inset of Fig. 5).

The $\langle d_i^2\rangle$ of immobile particles using definitions I, III, and IV are slightly larger but comparable to the $\langle d_i^2\rangle$ using definition II (see Fig. 5). We find for all definitions of immobility the same temperature dependence. Similarly the analogous figures for $T_{\mathrm{init}}=0.446$ are qualitatively the same.

To investigate further the heterogeneities we show in Fig. 6 the distribution of the vibrational amplitude normalized by

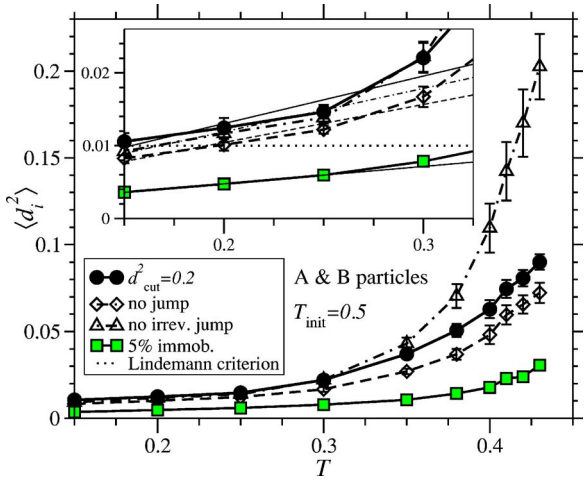

FIG. 5. (Color online) Same as Fig. 1 for immobile particles using definitions I–IV and for A and B particles. The inset shows an enlargement for low temperatures with linear fits through the origin and a line at $\langle d_i^2 \rangle = 0.01$ for the Lindemann criterion.

its average. The distribution of vibrational amplitudes has been predicted for the amorphous solid which results either from crosslinking macromolecules [2] or from cross-linking particles [3]—i.e., the gel state. In that context Q corresponds to the gel fraction and $\langle d_i^2 \rangle$ to the localization length squared. It was shown that the distribution of localization length obeys scaling in the critical regime of the transition from the fluid to the amorphous solid state which is a second-order equilibrium phase transition. The scaling function

$$\pi(\theta) = \pi\left(\frac{1/d_i^2}{\langle 1/d_i^2 \rangle}\right)$$

has been computed in mean-field theory and is given as the solution of

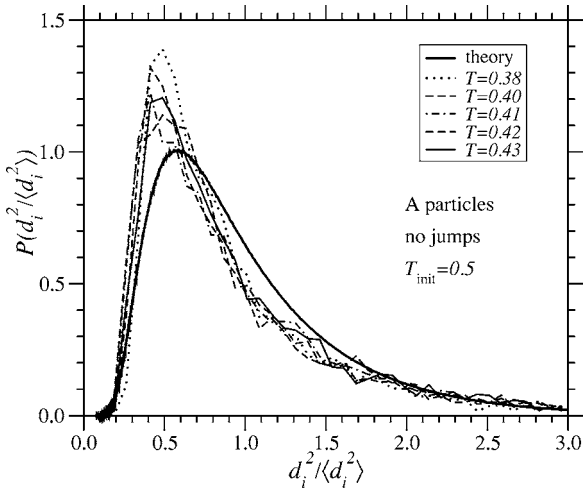

FIG. 6. Distribution of the normalized vibrational amplitude compared to a mean-field theory [3]. For the simulation data the definition III for immobility has been used and the distribution is shown for A particles.

$$(1-2\theta)\pi(\theta) = \theta^2\pi(\theta) + \int_0^\theta d\theta_1 \pi(\theta_1)\pi(\theta-\theta_1). \quad (5)$$

The theoretical results are in good agreement with results from numerical simulations of cross-linked macromolecular melts [21].

The two systems, binary Lennard-Jones glasses and cross-linked polymeric melts, have completely different microscopic dynamics, and the nature of the glass transition, if it exists, is not understood in contrast to the gelation transition. Nevertheless, it is an interesting open question to see whether the distribution of localization lengths $P(d_i^2)$ obeys scaling close to the glass transition and how it compares to the universal function of the gelation transition. The numerical solution to Eq. (5) is included as bold line in Fig. 6 which shows

$$P(d_i^2/\langle d_i^2 \rangle) = \theta\pi(\theta)\frac{\langle d_i^2 \rangle}{d_i^2}.$$

We find that indeed for temperatures $T \geqslant 0.38$, $P(d_i^2)$ depends on temperature only through the average squared localization length and that the normalized distribution compares reasonably well with the universal function of the gelation transition, as predicted by mean-field theory [2,3]. This agreement with theory is independent of the definition of immobility and independent of the history of initial configurations.

C. Cluster analysis

The vibrational amplitude has given us an estimate for the length scale of single-particle motion. In the rest of the paper we investigate how the immobile and mobile particles are spatially correlated with each other and how they are organized in clusters.

To do so we use definitions I–IV of immobility (see Sec. III) to select a subset of particles of the system. We stress again that immobility defined in this way is a time-persistent feature (on the time scale of the simulation run). We then choose a particular instant of time—the beginning of each production run—to identify nearest-neighbor connections among this subset of particles: particle j is defined to be a neighbor of particle i if their distance $|\mathbf{r}_{ij}| = |\mathbf{r}_i - \mathbf{r}_j|$ is smaller than the position of the first minimum $r_{\min}$ of the corresponding radial pair distribution function of the complete system ($r_{\min} = 1.4$ for AA, 1.2 for AB, and 1.07 for BB independent of temperature).

This definition of nearest-neighbor connections gives rise to K distinct clusters of immobile particles, with two particles belonging to the same cluster if they are connected. The clusters are numbered by $k = 1, 2, \ldots, K$ and we denote by $\mathcal{N}_k$ the kth cluster with N_k particles. The clusters of mobile particles are defined in complete analogy. However, in this case the identity of the clusters refers to a particular snapshot—usually the initial instant of time. In contrast the clusters of immobile particles are likely to be time-persistent structures.

To get a first idea of the organization of immobile particles into clusters we simply determine

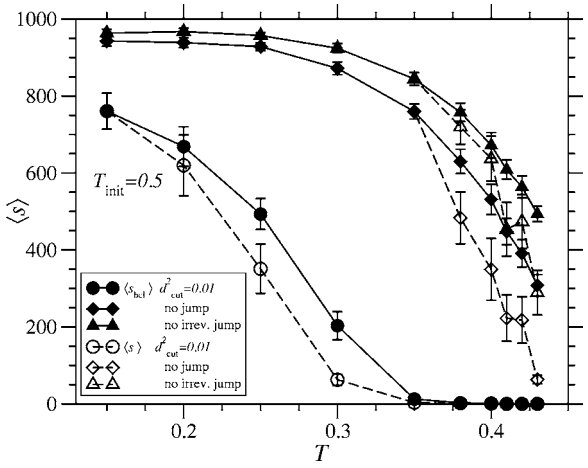

FIG. 7. Average number of cluster members s as a function of temperature. Shown are an average of s over only the biggest cluster of each independent configuration $\langle s_{\mathrm{bcl}}\rangle$ and an average over all clusters $\langle s\rangle$ are shown for definitions I, III, and IV.

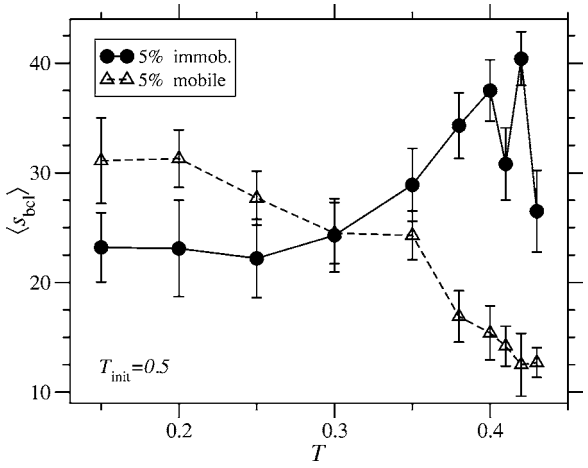

FIG. 8. Same as Fig. 7 but for definition II and only for $\langle s_{\mathrm{bcl}}\rangle$.

$$\langle s\rangle = \left\langle \frac{1}{K}\sum_{k=1}^{K} N_k \right\rangle, \tag{6}$$

i.e., the total number of immobile particles, $N_{immob}=\Sigma_{k=1}^{K}N_k$, divided by the total number of clusters K, averaged over initial conditions. Here and in the following $\langle\cdot\rangle$ denotes an average over initial conditions. In Fig. 7 we show $\langle s\rangle$ (open symbols) for the definitions I, III, and IV together with $\langle s_{\mathrm{bcl}}\rangle$ (solid symbols), where $s_{\mathrm{bcl}}=N_{k,\mathrm{bcl}}$ is the number of particles in the largest cluster. At the lowest temperatures almost all particles are immobile (see Figs. 3 and 4) and connected, so that there is only one large cluster and $\langle s\rangle=\langle s_{\mathrm{bcl}}\rangle$ is approximately given by the total number of particles. As the temperature increases the fraction of immobile particles decreases and the number of clusters decreases simultaneously so that $\langle s_{\mathrm{bcl}}\rangle > \langle s\rangle$. Definition IV ("no irreversible jump") gives rise to a larger $\langle s\rangle$ for immobile particles than definition III ("no jump"), since definition IV excludes fewer particles from the subset than definition III—namely, only irreversible instead of also reversible jumpers.

To disentangle the effects of spatial rearrangements and changing number of immobile particles, we use definition II with a *fixed* number of immobile particles.

Figure 8 shows $\langle s_{\mathrm{bcl}}\rangle$ for the 5% most mobile and 5% most immobile particles as a function of temperature. In the temperature range $0.25 \leqslant T \leqslant 0.4$ the 5% immobile particles cluster increasingly more together with increasing temperature. We interpret this such that immobile particles manage to stay immobile at larger temperatures by forming each other's cages most successfully by clustering together. The 5% most mobile particles, on the other hand, cluster more together at lower temperatures. A more cooperative motion allows the particles to be mobile at low temperatures.

This picture gets further support from the observation that with increasing temperature the number of clusters $\langle K\rangle$ increases for the 5% most mobile particles and decreases for the 5% most immobile ones (see Fig. 9). This temperature dependence is qualitatively the same for simulations with different histories ($T_{\mathrm{init}}=0.446$ and $T_{\mathrm{init}}=0.5$).

Another interesting question concerns the percolation properties of clusters of either immobile or mobile particles. We vary the percentage p of immobile particles and thereby the clusters $\mathcal{N}_k$ as well as the total number of clusters K. For a fixed temperature T we compute the fraction P_{perc} of the ten independent configurations with a percolating cluster of immobile particles. We define a cluster to be percolating if its maximum extension $r_\nu=\max|r_{i\nu}-r_{j_\nu}|$ between any pair of particles i and j satisfies $r_\nu > 8.0$ for any direction $\nu \in \{x,y,z\}$ [22]. As can be seen in the inset of Fig. 10 this fraction rises sharply from zero at a critical value p_c, which is approximately independent of temperature. A central quantity from percolation theory is the average cluster size, defined as

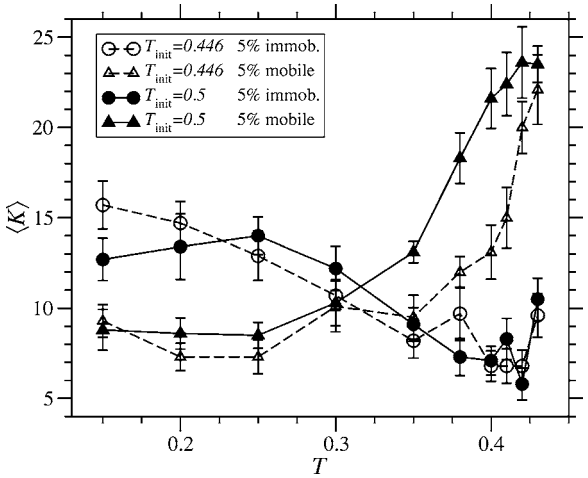

FIG. 9. Average number of clusters $\langle K\rangle$ as a function of temperature using definition II.

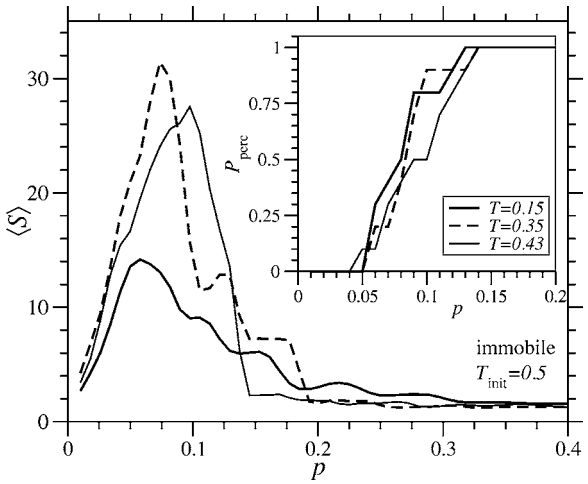

FIG. 10. The average cluster size $\langle S \rangle$ as a function of percentage p using definition II for immobility. The average is over all nonpercolating clusters and over independent initial configurations. The inset shows the fraction of percolating configurations as a function of p.

$$\langle S \rangle(p) = \left\langle \frac{\sum_s s^2 n_s(p)}{\sum_s s n_s(p)} \right\rangle \text{ with } n_s = \sum_{k=1}^{K} \delta_{N_k,s}. \tag{7}$$

Percolation theory predicts a divergence of $\langle S(p) \rangle$, as the percolation transition is approached from either side (excluding the percolating cluster for $p > p_c$). In our case we observe a strong increase of $\langle S \rangle$, a maximum around p_c, and a subsequent decrease for $p > p_c$ (see Fig. 10). The strong increase of $\langle S \rangle$ around p_c is reminiscent of a percolation transition with, however, a threshold value that is significantly lower than the corresponding value for hard spheres [23]. This may be due to the strong correlations between immobile particles in addition to the correlations due to the interaction potential $V(r)$. Furthermore, our analysis is severely hampered by the small size of our sample, which percolates much easier than a larger sample, so that p_c is underestimated.

The *spatial* extent of clusters of immobile and mobile particles can be quantified with the help of the radius of gyration. The latter is defined for a particular cluster $\mathcal{N}_k$:

$$R_G(\mathcal{N}_k) = \sqrt{\frac{1}{N_k} \sum_{i \in \mathcal{N}_k} (\mathbf{r}_i - \mathbf{r}_{c.m.})^2}, \tag{8}$$

with the center of mass of the cluster

$$\mathbf{r}_{c.m.} = \frac{1}{N_k} \sum_{i \in \mathcal{N}_k} \mathbf{r}_i. \tag{9}$$

To study the scaling of R_G as a function of the number of particles in a cluster s, we show in Fig. 11 a log-log plot of $R_G(\mathcal{N}_k)$ versus $s(\mathcal{N}_k)$ for all clusters $\mathcal{N}_k$ of all independent configurations. We find that approximately $R_G \propto s^{1/d_f}$ with a fractal dimension $d_f \approx 1.8$ (and similarly for the definitions II–IV). If the clusters were approximately straight lines, one would expect $d_f = 1.0$; if they were compact, $d_f = 3.0$. Our

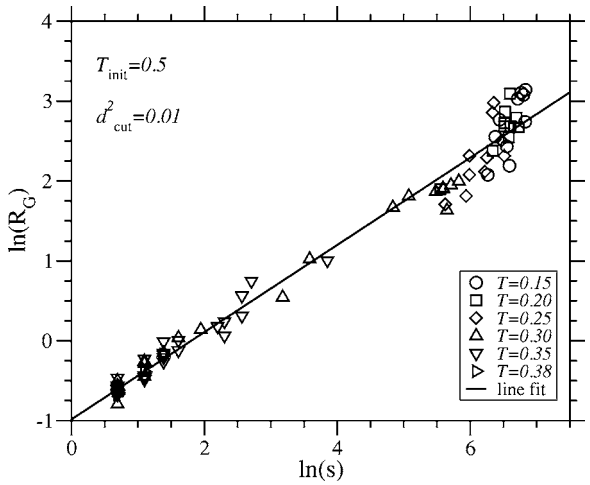

FIG. 11. Log-log plot of the radius of gyration, R_G, as a function of the number of cluster members s using definition I for immobility. The line is a linear fit with slope 0.55.

result points to fractal structures; however, this should be taken with a caveat since the clusters are too small to observe true asymptotic scaling behavior.

Next, we investigate the connectivity within single clusters. Since two sites have been defined to be connected if sufficiently close in space, the connectivity is not a purely topological feature, but gives us information about the shape of the clusters. A convenient measure, which does not require a large variety of cluster sizes, is the coordination number z. We define the average coordination number $z(\mathcal{N}_k)$ of a cluster $\mathcal{N}_k$ as

$$z(\mathcal{N}_k) = \frac{1}{N_k} \sum_{i \in \mathcal{N}_k} z_i, \tag{10}$$

where z_i is the number of neighboring particles $j \in \mathcal{N}_k$ of particle i. Figure 12 gives a plot of $\langle z_{bcl} \rangle = \langle z(\mathcal{N}_{bcl}) \rangle$, the average number of neighbors of particles in the biggest cluster averaged over independent initial configurations. We observe

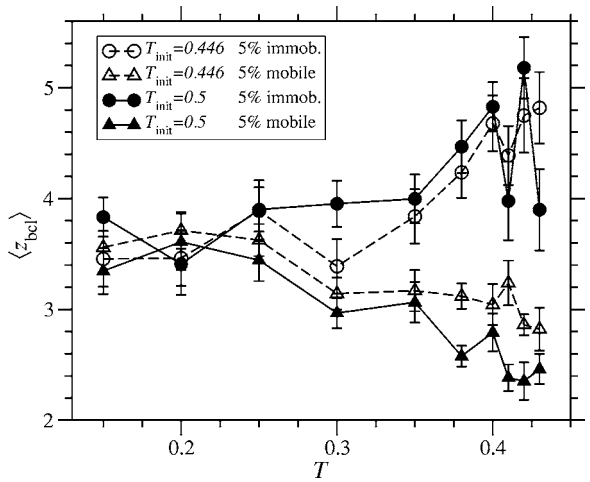

FIG. 12. Average coordination number of members of the biggest cluster $\langle z_{bcl} \rangle$ as a function of temperature using definition II.

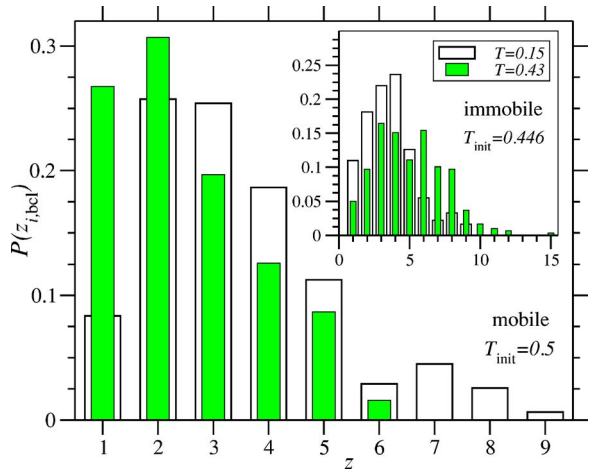

FIG. 13. (Color online) Distribution of coordination numbers $P(z_{i,\mathrm{bcl}})$ of the 5% fastest particles in the biggest cluster for simulations with $T_{\mathrm{init}}=0.5$. The inset shows $P(z_{i,\mathrm{bcl}})$ for the 5% slowest particles for simulations with $T_{\mathrm{init}}=0.446$.

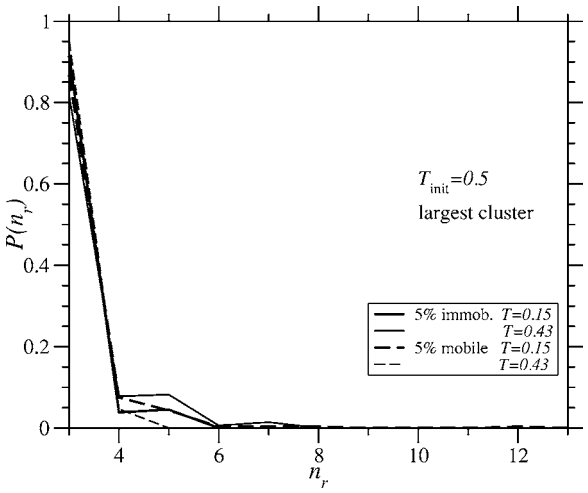

FIG. 14. Distribution of ring sizes $P(n_r)$ within the largest cluster of each independent configuration using definition II.

that $\langle z_{\mathrm{bcl}}\rangle$ is increasing for the 5% immobile particles with increasing temperature, independent of the history of the runs. The immobile particles block each other at larger temperatures by clustering more together and by forming more compact clusters. Clusters of mobile particles, on the other hand, become more elongated with increasing temperature. Although $\langle z_{\mathrm{bcl}}\rangle$ is not equal to 2 as it would be for strings, $\langle z_{\mathrm{bcl}}\rangle$ approaches 2.5 as $T\rightarrow T_g$. This is reminiscent of the results [9–11], where increasingly stringlike motion for mobile particles was observed as the glass transition is approached from *above*. (The authors of [9–11] use a slightly different definition of mobility than in this paper and define a string via velocity-velocity correlations.)

More information about the connectivity and the shape of the cluster can be found from the distribution of coordination numbers of the particles in the biggest cluster for each initial configuration $P(z_{i,\mathrm{bcl}})=P(z_{i\in\mathcal{N}_{\mathrm{bcl}}})$. Figure 13 illustrates that for low temperatures $z=3$ and $z=2$ are the most common coordination numbers of the mobile particles in the biggest cluster. However, for high temperatures $z=2$ dominates and the variance of the distribution is smaller, indicating stringlike clusters. In the case of the 5% immobile particles, on the other hand, the peak is at $z=4$ and the variance of $P(z_{i\in\mathcal{N}_{\mathrm{bcl}}})$ is strongly increasing with increasing temperature (see the inset of Fig. 13). This indicates increasingly more compact clusters with increasing temperature.

We finish our cluster analysis with ring statistics. Whereas ring analysis usually is applied to network forming glasses, it is here applied to the binary Lennard-Jones system, which is a fragile glass former [24]. In the following we call any path a set of nearest-neighbor connections. The most commonly used method, introduced by King [25], searches for rings by finding for each particle and any pair of its neighbors the shortest path between them. As pointed out by Franzblau [26], this definition has serious disadvantages such as not counting certain "intuitive" rings, which leads Franzblau to the "shortest-path" (SP) criterion: an SP ring contains for each pair of particles in the ring the shortest path between the pair in the cluster under consideration. We use the SP criterion and search algorithm of Franzblau to find within the largest cluster all rings $r=1,N_{r,\mathrm{bcl}}$ each of size n_r—i.e., with n_r connections.

Figure 14 shows the distribution $P(n_r)$ for the biggest cluster of the 5% immobile and 5% mobile particles. We find that rings are dominantly made up of three particles; only a few rings are longer. This means that in the case of the "stringier" mobile particle clusters, the clusters are mostly not closed rings.

In the case of immobile clusters using definitions I, III, and IV larger clusters are formed, leading to a larger average ring size

$$\langle n_{\mathrm{bcl}}\rangle=\left\langle\frac{1}{N_{r,\mathrm{bcl}}}\sum_{r=1}^{N_{r,\mathrm{bcl}}}n_r\right\rangle \tag{11}$$

(see Fig. 15). For low temperatures almost all particles are members of the biggest cluster of immobile particles and

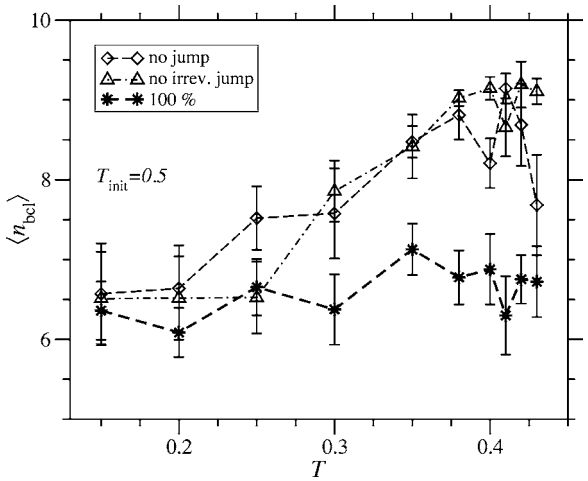

FIG. 15. Average ring size $\langle n_{\mathrm{bcl}}\rangle$ as a function of temperature using definitions III and IV and the comparison of $\langle n\rangle$ for the complete system (100%).

$\langle n_{\mathrm{bcl}} \rangle$ is therefore comparable to $\langle n \rangle$ of the whole system. For larger temperatures the clusters become more compact and on average larger ring sizes occur.

V. CONCLUSIONS

We investigate a binary Lennard-Jones system below the glass transition. To study the inhomogeneous structure of the glassy state quantitatively we focus on the most mobile and immobile particles. Since the identification of these is not unique—at least not in a simulation run of finite length—we test different definitions of immobility. The first two definitions are based on the vibrational amplitude, and the last two define a particle to be immobile if it is not jumping.

The length scales of single-particle motion vary strongly among the particles, giving rise to a broad distribution of vibrational amplitudes for mobile and immobile particles. The range of vibrational amplitudes increases as the glass transition temperature is approached from below: The system not only becomes more heterogeneous with increasing temperature, but also the range of length scales extends to much larger scales in the vicinity of the glass transition than at low temperatures. Focusing on the immobile particles only, we observe the distribution of vibrational amplitudes to follow a scaling plot close to the glass transition. It even compares reasonably well with a mean-field theory for the amorphous solid state, developed in the context of the gelation transition. Tentatively this may be taken as evidence for the recently suggested picture of the more general jamming transition [27], including both the gel transition and the glass transition.

To characterize the spatial arrangement and correlations among immobile and mobile particles, we identify clusters of particles, which are defined to be connected if their relative distance is smaller than a threshold value, given by the first minimum of the pair correlation function. Whereas for the immobile particles these clusters are approximately time persistent and hence characterize the static heterogeneity, the clusters of mobile particles are relevant for the dynamic heterogeneity of the glassy state.

If immobility is defined by the vibrational amplitudes or the jump characteristics, then the number of immobile particles increases strongly as the temperature is lowered. This effect dominates the statistics of cluster number, size, and shape. Baljon *et al.* [28] find similar results for thin polymer films by looking at the percolation probability of immobile monomers as a function of temperature. It is instructive to keep the number of immobile and mobile particles constant—namely, the $p\%$ particles with the smallest and largest vibrational amplitudes. The $p\%$ mobile particles, on the other hand, cluster more together at low temperatures and form more elongated stringlike clusters at larger temperatures. Similar strings have been found for the same system above the glass transition [4,5] and for a similar system above and slightly below the critical temperature [7]. These simulations and our results as well as experiments [11] point to stringlike clusters of mobile particles which grow close to the glass transition temperature, both when approached from above and when approached from below the glass transition. We find that with increasing temperature the $p\%$ immobile particles cluster more strongly together and form more compact clusters which allows the particles to block each other more effectively and to therefore stay immobile.

ACKNOWLEDGMENTS

K.V.L. gratefully acknowledges financial support from DFG Grant No. Zi 209/6-1. We thank W. Kob for input in the early stages of this work and B. Vollmayr-Lee for a careful reading of the manuscript.

[1] For review articles see R. Böhmer, Curr. Opin. Solid State Mater. Sci. **3**, 378 (1998); H. Sillescu, J. Non-Cryst. Solids **243**, 81 (1999); M. D. Ediger, Annu. Rev. Phys. Chem. **51**, 99 (2000).
[2] H. E. Castillo, P. M. Goldbart, and A. Zippelius, Europhys. Lett. **28**, 519 (1994); P. M. Goldbart, H. Castillo, and A. Zippelius, Adv. Phys. **45**, 393 (1996).
[3] K. Broderix, M. Weigt, and A. Zippelius, Eur. Phys. J. B **29**, 441 (2002).
[4] C. Donati, J. F. Douglas, W. Kob, S. J. Plimpton, P. H. Poole, and S. C. Glotzer, Phys. Rev. Lett. **80**, 2338 (1998).
[5] C. Donati, S. C. Glotzer, P. H. Poole, W. Kob, and S. J. Plimpton, Phys. Rev. E **60**, 3107 (1999).
[6] D. N. Perera and P. Harrowell, J. Chem. Phys. **111**, 5441 (1999).
[7] M. Vogel, B. Doliwa, A. Heuer, and S. C. Glotzer, J. Chem. Phys. **120**, 4404 (2004).
[8] V. Teboul, A. Monteil, L. C. Fai, A. Kerrache, and S. Maabou, Eur. Phys. J. B **40**, 49 (2004).
[9] S. C. Glotzer, and C. Donati, J. Phys.: Condens. Matter **11**, A285 (1999); Y. Gebremichael, T. B. Schrøder, F. W. Starr, and S. C. Glotzer, Phys. Rev. E **64**, 051503 (2001); M. Aichele, Y. Gebremichael, F. W. Starr, J. Baschnagel, and S. C. Glotzer, J. Chem. Phys. **119**, 5290 (2003); Y. Gebremichael, M. Vogel, and S. C. Glotzer, *ibid.* **120**, 4415 (2004).
[10] M. Vogel and S. C. Glotzer, Phys. Rev. E **70**, 061504 (2004).
[11] E. R. Weeks, J. C. Crocker, A. C. Levitt, A. Schofield, and D. A. Weitz, Science **287**, 627 (2000).
[12] W. Kob and H. C. Andersen, Phys. Rev. Lett. **73**, 1376 (1994); Phys. Rev. E **51**, 4626 (1995); **52**, 4134 (1995).
[13] K. Vollmayr-Lee, J. Chem. Phys. **121**, 4781 (2004).
[14] It has been shown in [15] (for an (NpT) cooling process) that this cooling rate is sufficiently slow that the system never falls out of equilibrium during the cooling process from $T=3.0$ to $T=0.5$.
[15] K. Vollmayr-Lee, W. Kob, and K. Binder, J. Chem. Phys. **105**, 4714 (1996).
[16] W. Kob and J.-L. Barrat, Phys. Rev. Lett. **78**, 4581 (1997).
[17] J.-L. Barrat and W. Kob, Europhys. Lett. **46**, 637 (1999).
[18] K. Vollmayr-Lee, W. Kob, K. Binder, and A. Zippelius, J.

Chem. Phys. **116**, 5158 (2002).
[19] The choice of $\sqrt{20}$ for the coefficient was made after the investigation by eye of many representative single trajectories. For a significantly smaller coefficient fluctuations would be picked up as jump events and for a significantly larger coefficient jumps would not be detected.
[20] Here and for all other figures error bars are determined solely via the average over the ten independent configurations.
[21] S. J. Barsky and M. Plischke, Phys. Rev. E **53**, 871 (1996); M. Plischke and S. J. Barsky, *ibid.* **58**, 3347 (1998); S. Barsky and M. Plischke, *ibid.* **60**, 4528 (1999).
[22] For the definition of r_ν as well as for R_G (see below) we have to make sure to eliminate the effect of periodic boundary conditions. We therefore first unwrap each cluster; i.e., periodic images are chosen such that all neighboring particles satisfy directly $r_{ij} \leqslant r_{\min}$.
[23] D. Stauffer, Phys. Rep. **54**, 1 (1979); Y. C. Chiew and E. D. Glandt, J. Phys. A **16**, 2599 (1983).
[24] W. Kob, J. Phys.: Condens. Matter **11**, R85 (1999).
[25] S. V. King, Nature (London) **213**, 1112 (1967).
[26] D. S. Franzblau, Phys. Rev. B **44**, 4925 (1991).
[27] A. J. Liu and S. R. Nagel, Nature (London) **396**, 21 (1998).
[28] A. R. C. Baljon, J. Billen, and R. Khare, Phys. Rev. Lett. **93**, 255701 (2004).